Single vs. Multiple Transponders for Radio Tomography of Asteroids

S. Pursiainen[†‡] and M. Kaasalainen[†]

† Department of Mathematics, Tampere University of Technology, Tietotalo Building, FI-33720 Tampere, Finland.

‡ Department of Mathematics and Systems Analysis, Aalto University, P.O. Box 11100, FI-00076 Aalto, Finland.

Email: sampsa.pursiainen@aalto.fi

TAMPERE UNIVERSITY OF TECHNOLOGY

Finnish Centre of Excellence in Inverse Problems Research

Introduction

The purpose of this study was to advance numerical methods for radio tomography in which asteroid's internal electric permittivity distribution is to be recovered from radio frequency data gathered by an orbiter. The tomography approach examined was closely related to that of the CONSERT experiment [1] aiming at recovery of a comet nucleus structure as a part of the ROSETTA mission. The focus was on signal generation via multiple sources (transponders) providing one potential, or even essential, scenario to be implemented in a challenging *in situ* measurement environment and within tight payload limits. The permittivity was reconstructed with a combination of the iterative alternating sequential (IAS) inverse algorithm [2] and finite-difference time-domain (FDTD) forward simulation [3]. Single and multiple source scenarios were compared in two-dimensional localization of permittivity anomalies.

Forward Model and Simulation

The applied forward model predicted the electric potential ϕ in the set $[0,T]\times\Omega$ in which $[0,T]$ was a time interval and the spatial part Ω was assumed to contain the target asteroid together with orbiter's trajectory. The parameters given included a real-valued relative electric permittivity ε_r, real conductivity distribution σ, as well as the initial conditions $\phi|_{t=0}=\phi_0$ and $(\partial\phi/\partial t)|_{t=0}=u_1$. The electric potential was assumed to satisfy a hyperbolic wave equation the form

$$\varepsilon_r\frac{\partial^2\phi}{\partial t^2}+\sigma\frac{\partial\phi}{\partial t}-\Delta_{\vec{x}}\phi=\mathtt{f}\quad\text{for all}\quad(t,\vec{x})\in[0,T]\times\Omega.$$

The forward model was simulated via the FDTD method [3] and linearized around a background permittivity resulting in $\mathbf{y}=\overline{\mathbf{y}}_{bg}+\mathbf{L}\mathbf{x}+\mathbf{n}$ with $\mathbf{L}$ denoting a matrix, $\mathbf{y}$ and $\overline{\mathbf{y}}_{bg}$ actual and background time derivative $(\partial\phi/\partial t)$ data, $\mathbf{x}$ perturbation, and $\mathbf{n}$ total noise (TN). Examples of 3D wave propagation for single and six sources have been included in Figure 1.

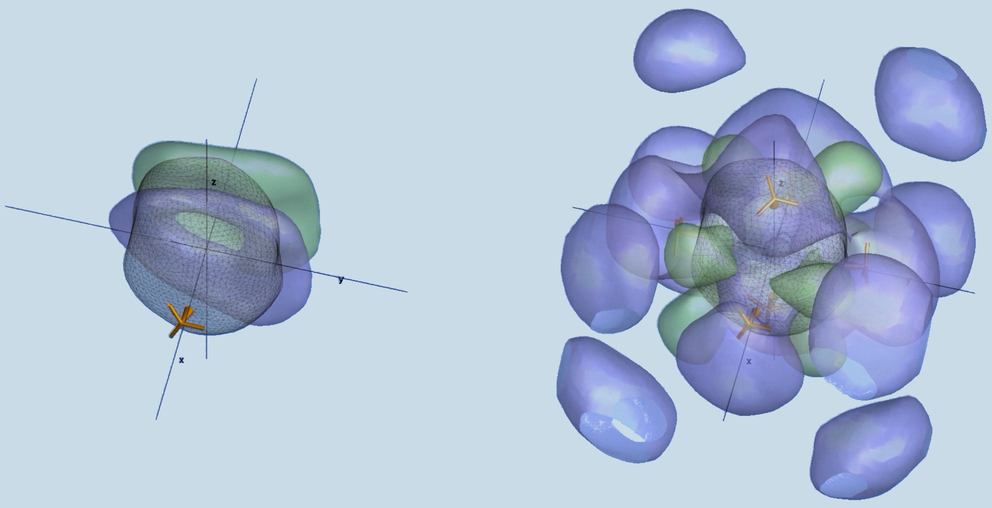

Figure 1: Examples of signal propagation in 3D illustrating the positive (green) and negative (blue) isosurface for single (left) and six (right) sources or transponders visualized by the three-branch antennas.

Inverse Model

The inverse model was a hierarchical Bayesian one. A reconstruction was found by estimating the maximizer (MAP) of a joint posterior density of the permittivity perturbation $\mathbf{x}$ and a hyperparameter $\mathbf{z}$. The posterior was formed as the product $p(\mathbf{x},\mathbf{z}\mid\mathbf{y})\propto p(\mathbf{y}\mid\mathbf{x})p(\mathbf{x}\mid\mathbf{z})p(\mathbf{z})$ of a conditional prior $p(\mathbf{x}\mid\mathbf{z})$, hyperprior $p(\mathbf{z})$ and likelihood $p(\mathbf{y}\mid\mathbf{x})$ with the last one following from the distribution $p(\mathbf{n})$ of TN via substitution $\mathbf{n}=\mathbf{y}-\overline{\mathbf{y}}_{bg}-\mathbf{L}\mathbf{x}$. Both $p(\mathbf{n})$ and the conditional prior were zero mean Gaussian with a diagonal covariance matrix of the form $(2\nu^2)^{-1}I$, and $\mathbf{D}_\mathbf{z}=\mathrm{diag}(z_1,z_1,\ldots,z_n)$, respectively. To maximize the posterior, the following iterative alternating sequential (IAS) algorithm [2] was utilized:

(1) Set $\mathbf{z}_0=(\theta_0,\theta_0,\ldots,\theta_0)$, $i=1$ and iterate between the following two steps;

(2) Find $\mathbf{x}^{(i)}=\mathrm{argmax}\{p(\mathbf{x}\mid\mathbf{y},\mathbf{z}^{(i-1)})\}$;

(3) Find $\mathbf{z}^{(i)}=\mathrm{argmax}\{p(\mathbf{z}\mid\mathbf{y},\mathbf{x}^{(i)})\}$ and set $i=i+1$.

The maximizer estimated was of the form $\mathbf{x}^{(g)}=\mathrm{argmin}\{\|\mathbf{y}-\overline{\mathbf{y}}_{bg}-\mathbf{L}\mathbf{x}\|_2^2+\delta\|\mathbf{x}\|_1\}$.

Numerical Experiments

Numerical experiments concerned a 2D square-shaped spatial domain Ω composed of disjoint subsets Ω_0 – Ω_3 (Figure 2). The goal was to detect from Ω_0 a perturbation formed by three separate permittivity anomalies 1–3 supported on Ω_1. Signal sources were placed on the outer boundary of Ω_0. The data was gathered in Ω_2 along a circular path enclosing Ω_0. Subdomain Ω_3 formed a perfectly matched layer. Relative permittivity ε_r of the background Ω_0 was set to be 4 (e.g. granite, dunite, kaolinite) and that of anomalies either (A) 25 %, (B) 50 % or (C) 75 % lower compared to the background. Conductivity was given assumed to have an unknown (latent) distribution $\sigma=5\varepsilon_r$. The diameter of Ω_0 varied between 90 and 135 m. A Blackman-Harris type pulse with duration 170 ns wand center frequency of 12 MHz was used as a signal source. TN consisted of zero mean Gaussian white noise filtered close to the signal frequency. Both fair $\nu=0.8$ and high $\nu=1.6$ TN standard deviation levels were examined.

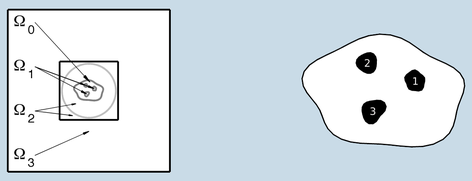

Figure 2: On left: Subdomains Ω_0–Ω_3. On right: Anomalies 1–3 forming Ω_1.

Results

Comparison (I): Total Noise

Figure 3 compares the effect of fair and high TN in reconstructing the slight 25 % perturbation (A). When recovered with fair TN, anomalies 1–3 were visible in a overlapping set $\mathcal{S}$ (overlap of actual and detected anomalies with identical area) with all source counts. Anomaly 2 was judged as not detected in the case of high TN and a single source. Otherwise, 1–3 were regarded as detectable based on $\mathcal{S}$. Single and two sources led to unbalanced mutual contrast between the anomalies: for example, anomaly 1 closest to the signal source was dominant in the reconstructions produced with a single source. The relative difference in relative overlapping area (ROA) between fair and high TN had a declining tendency (14 %, 18 %, 11 %, 3 %) as the source count increased, indicating improving noise tolerance.

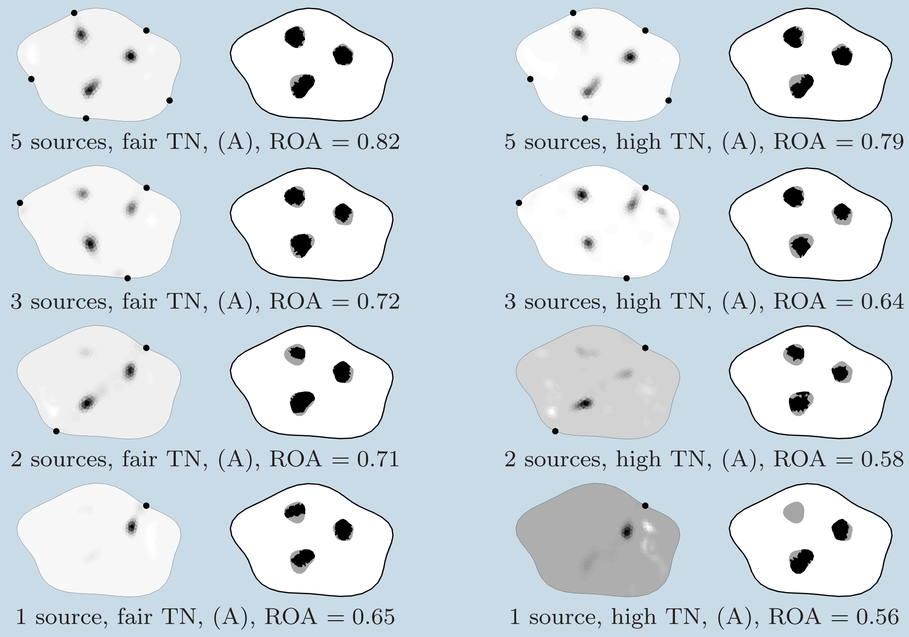

Figure 3: Comparison (I): Reconstructions of 25 % perturbation (A) with fair (left) and high (right) TN. The number of sources from top to bottom row is 5,3,2, and 1, respectively, with the locations indicated by black dots. Each visualization shows a reconstruction (left) and an overlapping set $\mathcal{S}$ (right).

Comparison (II): *A Priori* Information

Figure 4 compares reconstructions of the stronger 50 % and 75 % perturbations (B) and (C) in the case of fair TN. Based on visual judgement, two and five sources were needed to detect anomaly 3 of (B) and (C) whereas anomalies 1–2 were detectable with each tested source count. Five sources led to the best reconstructions both visually and in terms of ROA. The recovered anomalies of (C) were somewhat displaced towards the boundary of $\Omega_0\cup\Omega_1$ resulting into a relatively low ROA.

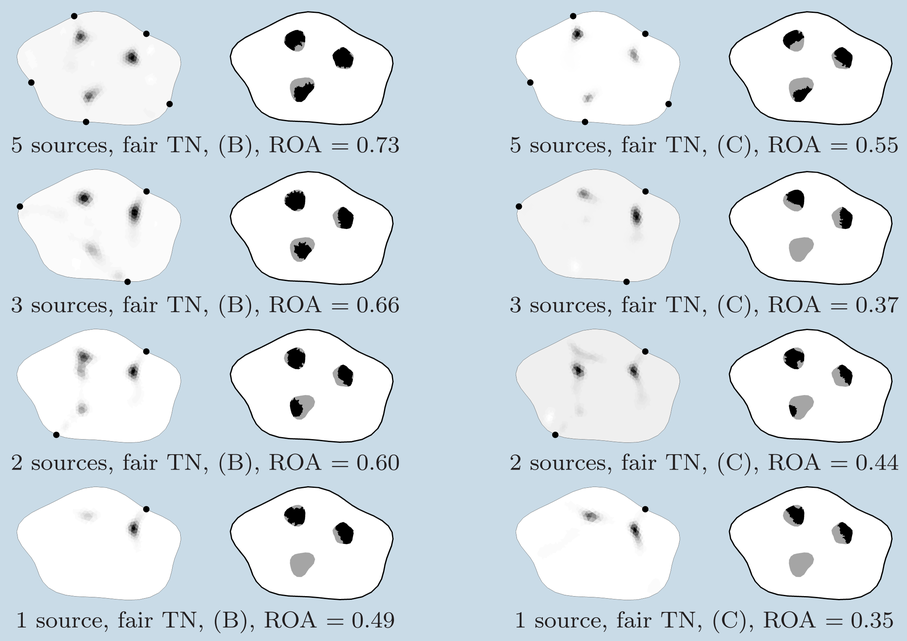

Figure 4: Comparison (II): Reconstructions of 50 % and 75 % perturbations (B) (left) and (C) (right) with fair TN. The number of sources from top to bottom row is 5,3,2, and 1, respectively, with the locations indicated by black dots. Each visualization shows a reconstruction (left) and an overlapping set $\mathcal{S}$ (right).

Conclusions

The robustness of the inverse results was observed to improve significantly along with the source count regarding both mutual contrast of the recovered anomalies and also tolerance to total noise (TN). Multiple sources were found to be necessary to distinguish (in 2D) three separate anomalies with permittivity less or equal than half of the background value, relevant in recovery of internal cavities. Of the applied TN levels, the best reconstruction quality was obtained with the fair one the peak signal-to-noise ratio of which with respect to $\|\mathbf{y}\|$ was -15.9 – -12.6 dB. As for the signal quality, the inverse results were inferred to have been essentially determined by the strongest spikes of the difference data $\mathbf{y}-\overline{\mathbf{y}}_{bg}$.

References

[1] Kofman W. et al. (1998) Space Sci. Rev., 128, 413 – 432.

[3] Pursiainen S.; Kaasalainen M. (2013) Planet. Space Sci., 82–83, 84–98.

[2] Schneider J. B., (2013) Understanding the FDTD Method, Available online.